BIOCHEMISTRY
including biophysical chemistry & molecular biology
Article

Biochemistry **2009,** *48,* 11715–11723 11715
DOI: 10.1021/bi901524q

Evidence of Kinetic Control of Ligand Binding and Staged Product Release in MurA (Enolpyruvyl UDP-GlcNAc Synthase)-Catalyzed Reactions[†,‡]

Sean G. Jackson,[∥,⊥] Fuzhong Zhang,[§] Paul Chindemi,[§] Murray S. Junop,[∥,⊥] and Paul J. Berti*[,§,∥]

[§]*Department of Chemistry and Chemical Biology, and* [∥]*Department of Biochemistry and Biomedical Sciences, and* [⊥]*Michael G. DeGroote Institute for Infectious Disease Research, McMaster University, 1280 Main Street West, Hamilton, Ontario L8S 4M1, Canada*

Received August 31, 2009; Revised Manuscript Received November 8, 2009

ABSTRACT: MurA (enolpyruvyl UDP-GlcNAc synthase) catalyzes the first committed step in peptidoglycan biosynthesis. In this study, MurA-catalyzed breakdown of its tetrahedral intermediate (THI), with a k_{cat}/K_M of 520 M^{-1} s^{-1}, was far slower than the normal reaction, and 3×10^5-fold slower than the homologous enzyme, AroA, reacting with its THI. This provided kinetic evidence of slow binding and a conformationally constrained active site. The MurA cocrystal structure with UDP-*N*-acetylmuramic acid (UDP-MurNAc), a potent inhibitor, and phosphite revealed a new "staged" MurA conformation in which the Arg397 side chain tracked phosphite out of the catalytic site. The closed-to-staged transition involved breaking eight MurA·ligand ion pairs, and three intraprotein hydrogen bonds helping hold the active site loop closed. These were replaced with only two MurA·UDP-MurNAc ion pairs, two with phosphite, and seven new intraprotein ion pairs or hydrogen bonds. Cys115 appears to have an important role in forming the staged conformation. The staged conformation appears to be one step in a complex choreography of release of the product from MurA.

MurA[1] (enolpyruvyl UDP-GlcNAc synthase) is an antimicrobial target that is inhibited by the antibiotic fosfomycin (*1*, *2*). It converts phosphoenolpyruvate (PEP) and the 3-hydroxyl group of UDP-*N*-acetylglucosamine (UDP-GlcNAc) into enolpyruvyl UDP-*N*-acetylglucosamine (EP-UDP-GlcNAc) and inorganic phosphate (P_i) in the first committed step of peptidoglycan biosynthesis (Scheme 1). MurB then reduces the enolpyruvyl group to form UDP-*N*-acetylmuramic acid (UDP-MurNAc). UDP-MurNAc inhibits MurA with a K_i of 0.9 μM (*3*), which is below its physiological concentration of 5−35 μM (*4*), implying a possible physiological role in regulating peptidoglycan biosynthesis.

MurA's mechanism (*5*−*12*) and structure (*2*, *11*−*20*) have been characterized extensively. It is homologous with AroA, an enzyme in the shikimate biosynthetic pathway that catalyzes essentially the same reaction as MurA (*21*, *22*). In the AroA-catalyzed reaction, PEP and the 5-hydroxyl group of shikimate 3-phosphate are converted to enolpyruvyl shikimate 3-phosphate and P_i. Both enzymes catalyze an addition−elimination reaction which proceeds through a tetrahedral intermediate (THI) (*8*, *21*). The THIs were identified as true catalytic intermediates on the basis of their kinetic competence; that is, they are formed and degraded fast enough under pre-steady state conditions to account for the overall reaction rate. AroA THI is an excellent AroA substrate, with a k_{cat}/K_M of 1.4×10^8 M^{-1} s^{-1} (*23*, *24*).

AroA's two domains move as essentially rigid units in crystal structures, being hinged at the base of the active site cleft located at the domain interface (*15*, *25*−*27*). The open, unliganded form converts to the closed, ligand-bound form through rotation of the domains. The nearly diffusion rate-limited rate of THI breakdown demonstrates that this motion is rapid. The MurA crystal structures, on the other hand, imply a more limited conformational repertoire, with conformational changes being largely limited to the active site loop, from P112 to P121 (*Escherichia coli* MurA numbering), which closes over the catalytic site like a flap. However, as crystallography is intrinsically static, the rate of conversion between open and closed forms is not known, nor is the functional significance, if any, of the more limited conformational changes.

The active site loop contains the cysteine residue that is alkylated by fosfomycin, C115 (*28*). C115 is important for catalysis, as all mutations except that to Asp inactivate MurA (*12*, *16*, *29*). *E. coli* MurA_C115D is active, with a k_{cat} at its optimal pH higher than that of the wild type (*29*), and some bacterial species naturally contain Asp at this position (*29*, *30*). C115 has been proposed to act as a general acid catalyst, protonating C3 of PEP prior to nucleophilic attack by UDP-GlcNAc to form the THI (*29*). It is distant from C3 in most crystal structures (*15*, *16*, *19*, *20*) but approaches the PEP binding site in a fosfomycin-inhibited structure (*13*). It must also approach the PEP binding site when MurA forms a covalent phospholactoyl adduct with PEP (Scheme 2) (*31*). This occurs at

[†]This work was supported by Canadian Institutes of Health Research (CIHR) Operating Grants MOP-64422 (P.J.B.) and MOP-89903 (M.S.J.) and a CIHR CGS scholarship to S.G.J.

[‡]The structure factor amplitudes and the refined coordinates of the MurA·UDP-MurNAc·phosphite structure have been deposited in the Protein Data Bank as entry 3ISS.

*To whom correspondence should be addressed. Telephone: (905) 525-9140, ext. 23479. Fax: (905) 522-2509. E-mail: berti@mcmaster.ca.

[1]Abbreviations: AroA, enolpyruvyl shikimate 3-phosphate; EP-UDP-GlcNAc, enolpyruvyl uridine diphosphate *N*-acetylglucosamine; MurA, EP-UDP-GlcNAc synthase; PDB, Protein Data Bank; PEP, phosphoenolpyruvate; P_i, inorganic phosphate; rmsd, root-mean-square deviation; THI, tetrahedral intermediate; UDP-GlcNAc, uridine diphosphate *N*-acetylglucosamine; UDP-MurNAc, uridine diphosphate *N*-acetylmuramic acid.

Published on Web 11/09/2009

Scheme 1

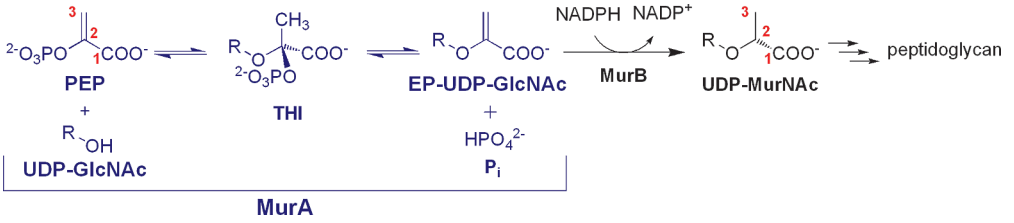

Scheme 2

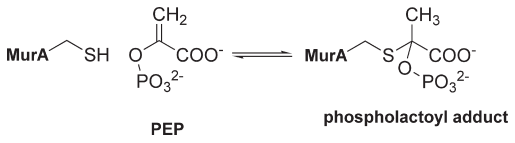

a rate approaching that of THI formation, implying that C115 approaches PEP in its normal binding site, as nucleophilic attack at C2 without prior, or simultaneous, protonation of C3 would not be possible (*32*). Recent kinetic and structural evidence has also strongly implicated C115 in product release (*16*). The C115S mutant crystallized as a complex with products EP-UDP-GlcNAc and P_i. It was capable of catalyzing only a single turnover because, apparently, it did not release its products. C115's proposed roles as a general acid catalyst and in product release are not mutually exclusive, and it could play both roles.

In this study, MurA was crystallized in a MurA·UDP-MurNAc·phosphite (HPO_3H^-) complex to elucidate enzyme·inhibitor interactions. The crystal structure revealed a new, "staged" protein conformation that illustrates the choreography of product release and provides further evidence of C115's role in product release. The kinetics of MurA-catalyzed THI breakdown provide functional evidence of the kinetic relevance of MurA's conformationally restricted active site.

EXPERIMENTAL PROCEDURES

General. Wild-type *E. coli* MurA was overexpressed and purified as described previously (*3*, *33*, *34*). The protein concentration was determined from A_{280} using an ε_{280} of 2.45×10^4 M^{-1} cm^{-1}, and the concentration of active protein was determined by titration of its activity with fosfomycin (*28*, *35*). UDP-MurNAc (*3*), [1-^{14}C]PEP (*3*), [1-^{14}C]THI (*33*), and 2-amino-6-mercapto-7-methylpurine ribonucleoside (MESG) (*36*) were synthesized as described previously. Pyruvate kinase, purine nucleoside phosphorylase (PNP), and other reagents were purchased from Sigma-Aldrich.

THI Breakdown and Partitioning. The rate of MurA [1-^{14}C]THI breakdown by MurA was monitored by the conversion of [1-^{14}C]THI to [1-^{14}C]EP-UDP-GlcNAc and [1-^{14}C]PEP (which was then converted to [1-^{14}C]pyruvate by pryuvate kinase). THI partitioning, i.e., the ratio of forward to reverse reaction products, was determined as (eq 1)

$$f(\mathrm{PEP}) = \frac{[[1\text{-}^{14}\mathrm{C}]\mathrm{PEP}]}{[[1\text{-}^{14}\mathrm{C}]\mathrm{PEP}] + [[1\text{-}^{14}\mathrm{C}]\mathrm{EP}\cdot\mathrm{UDP}\cdot\mathrm{GlcNAc}]} \quad (1)$$

Because THI breakdown was so slow, it was necessary to prevent the overall MurA reaction from interconverting [1-^{14}C]PEP and [1-^{14}C]EP-UDP-GlcNAc, which would have altered the partitioning results. This was done by consuming the product [1-^{14}C]PEP with pyruvate kinase and consuming P_i with PNP (Figure 1). Reaction mixtures (200 μL) contained 4 μM [1-^{14}C]THI (7000 cpm ^{14}C), 1 mM ADP, 0.13 mM MESG, 0.5 unit of pyruvate kinase, 0.3 unit of PNP, and 20−200 μM MurA in 1 mM $MgCl_2$, 15 mM KCl, and 50 mM Tris-HCl or HEPES-HCl (pH 7.5). Reactions were quenched after 15−45 min via addition of 200 mM KOH, and then mixtures were extracted repeatedly with chloroform until no more protein precipitated. The quenched reaction mixture was separated on a Mono Q anion exchange column (5 mm × 50 mm, GE Healthcare) in a gradient of 10 to 500 mM NH_4HCO_3 (pH 10.0) over 15 column volumes at a rate of 0.5 mL/min. Fractions of 0.5 mL were collected into scintillation vials; 20 mL of Liquiscint (National Diagnostics) scintillation fluid was added, and ^{14}C radioactivity was counted for 2 × 5 min. [1-^{14}C]PEP was given by [1-^{14}C]pyruvate, having been converted by pyruvate kinase. These experiments were also conducted at pH 5.0 using 50 mM ammonium acetate and at pH 10.0 using 50 mM CAPS buffer.

Protein Crystallization. MurA was further purified for crystallization. It was diluted 4-fold with buffer A [50 mM Tris-HCl (pH 8.0) and 2 mM dithiothreitol] and applied to a HiTrap QP-Sepharose HP ion exchange column (5 mL column volume, GE Healthcare). It was eluted with a gradient from buffer A to buffer B (buffer A with 0.5 M NaCl) over 24 column volumes in 120 min. The buffer was exchanged into 50 mM Tris-HCl (pH 8.0), 150 mM NaCl, and 2 mM dithiothreitol using a HiPrep 26/10 desalting column (53 mL column volume, GE Healthcare) at a flow rate of 8 mL/min and then concentrated to 5.0 mg/mL using a centrifugal filter. Sodium dodecyl sulfate−polyacrylamide gel electrophoresis (SDS−PAGE) indicated that MurA was >95% pure.

Crystallization and Data Collection. MurA was crystallized in the presence of sodium phosphite and UDP-MurNAc using the hanging drop vapor diffusion method under the following conditions. A 2 μL drop containing 1 μL of 5.0 mg/mL MurA with 0.5 mM sodium phosphite and 1.25 mM UDP-MurNAc and 1 μL of 0.1 M sodium MES (pH 6.5), 0.2 M ammonium sulfate, and 27% polyethylene glycol 5000 monomethyl ether was dehydrated over 500 μL of 0.5 M ammonium sulfate and incubated at 20 °C. Rectangular, block-shaped crystals were harvested and frozen in liquid nitrogen. Data were collected to a resolution of 2.5 Å at a wavelength of 1.0 Å at beamline X8C of the Brookhaven National Laboratory using a ADSC Quantum 4R CCD X-ray detector. The *D*trek* program suite (*37*) was used to process the data.

Structure Determination and Model Refinement. The MurA·UDP-MurNAc·phosphite crystal structure was solved by molecular replacement using *Phaser* (*38*) as part of the *Phenix* program suite (*39*). The molecular replacement search model was a monomer from the complex of *E. coli* MurA with fluoro-THI (FTHI) (PDB entry 1A2N), a closed conformation structure. FTHI was removed from the search model prior to molecular

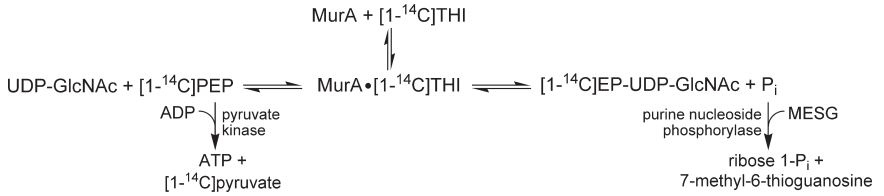

FIGURE 1: MurA THI partitioning. Breakdown of MurA THI to reactants, UDP-GlcNAc and PEP, or products, EP-UDP-GlcNAc and P_i, was much slower than the overall reaction of reactants to products. To determine the correct partitioning value, *f*(PEP), we used pyruvate kinase and purine nucleoside phosphorylase to consume all PEP and P_i, respectively, formed during THI breakdown, thereby preventing the overall MurA reaction.

replacement. Iterative cycles of model building and refinement were conducted using *WinCoot* (*40*) and *Phenix refine* (*39*), respectively. Noncrystallographic symmetry (NCS) and translation, libration, and screw-rotation (TLS) restraints were utilized during refinement. Protein structure figures were generated using *PyMol* (DeLano Scientific LLC).

RESULTS

MurA THI Breakdown. MurA-catalyzed THI breakdown had a second-order rate constant (k_{cat}/K_M) of 520 ± 240 M^{-1} s^{-1} at pH 7.5. It was higher at pH 5.0 (6000 ± 3000 M^{-1} s^{-1}) and, in a single determination, 570 M^{-1} s^{-1} at pH 10.0. This was 3×10^5-fold slower than the reaction of AroA with its THI, where $k_{cat}/K_M = 1.4 \times 10^8$ M^{-1} s^{-1} (*23*).

The mechanism of THI breakdown was investigated using *f*(PEP), the fraction of total THI that returned to reactants rather than going forward to products (Figure 1) (*23*). THI breakdown was so slow that the reactants and products were enzymatically equilibrated with each other faster than THI broke down, obscuring the value of *f*(PEP). This was prevented by the addition of pyruvate kinase to consume PEP, and PNP to consume P_i. With this system in place, *f*(PEP) was 0.22 ± 0.01, and it did not vary between pH 5.0 and 10.0.

MurA·UDP-MurNAc·Phosphite Crystal Structure. The MurA·UDP-MurNAc·phosphite complex crystallized with 12 protein molecules per asymmetric unit (Table 1). MurA crystal forms with 1−16 protein molecules in the asymmetric unit have been observed (Table 2); nevertheless, it appears to be a monomer in solution, even at high concentrations (*5*), so the number of molecules per asymmetric unit is not thought to be physiologically relevant. The molecular replacement search model was a closed conformation structure, *E. coli* MurA·FTHI, so the staged conformation observed here is not a result of bias imposed by the model. Residue N67 was modeled as isoaspartate (Asi), as observed previously (*15*). Each of the 12 MurA monomers adopted the staged conformation (see below) with a single UDP-MurNAc and phosphite ligand in the active site. The electron density for UDP-MurNAc in each of the 12 monomers was well-ordered.

Given the 2.50 Å resolution of the data, the exact orientation of phosphite was sometimes unclear. Most phosphite ions made some combination of two of three possible contacts, with the remaining oxygen directed toward solvent. The three MurA·phosphite contacts were with the R397 side chain, the R91 backbone NH group, and the C115 Sγ atom. The exception was chain I in which phosphite made all three contacts (Figures 2 and 5). In chain I, the electron density clearly indicated phosphite, though in some chains with less well-defined electron density, it was not possible to definitively rule out sulfate as the ligand. Finding phosphite in the active site in spite of its 400-fold lower concentration (0.5 mM phosphite vs 200 mM sulfate) is consistent with a previous study that did not find any interaction of sulfate with *E. coli* MurA or AroA (*34*).

Table 1: X-ray Data Collection and Refinement Statistics for the MurA·UDP-MurNAc·Phosphite Complex (PDB entry 3ISS)

Data Collection	
wavelength (Å)	1.0
space group	*P*1
unit cell parameters	
a, *b*, *c* (Å)	84.5, 120.9, 139.7
α, *β*, *γ* (deg)	111.5, 104.4, 90.2
no. of molecules per asymmetric unit	12
resolution range (Å)	47.48−2.50 (2.59−2.50)[a]
no. of unique reflections	167352
data redundancy	4.15 (4.18)[a]
completeness (%)	97.6 (97.3)[a]
$I/\sigma(I)$	7.0 (2.9)[a]
R_{merge} (%)	11.7 (43.5)[a]
Model and Refinement	
resolution range (Å)	47.48−2.50 (2.59−2.50)[a]
R_{work} (%)	0.221
R_{free} (%)	0.253
no. of reflections	167293
cutoff criterion [$F_{obs}/\sigma(F_{obs})$]	1.96
no. of amino acid residues/atoms	5016/37596
no. of ligand/ion atoms	576
no. of waters	853
rmsd for bond lengths (Å)	0.011
rmsd for bond angles (deg)	1.2
average *B* factor (Å^2)	46.8

[a]Data for the highest-resolution shell are shown in parentheses.

NCS and TLS restrained structure refinement resulted in a model with *R* and R_{free} values of 22.1 and 25.3%, respectively, and reasonable stereochemistry, with 92% of the 5004 residues having φ and ψ angles in the most favorable region.

DISCUSSION

MurA THI as a Substrate. The MurA X-ray crystal structures suggest limited flexibility, but with the caveat that crystal structures provide a static view of molecules that are dynamic in solution. Other experimental techniques provide clear evidence of conformational changes upon ligand binding, including small-angle X-ray scattering and fluorescence titrations (*5*), reactivity with fosfomycin (*41*), and proteolytic susceptibility (*42*), but no clear evidence whether they are kinetically important for catalysis. There is some anecdotal evidence of kinetically controlled ligand release, including the need to urea-denature MurA to dissociate UDP-GlcNAc (*31*), and the fact that the MurA·UDP-MurNAc complex did not dissociate through five protein purification steps (*3*).

Table 2: All MurA Crystal Structures

conformation	description	no. of molecules per asymmetric unit	PDB entry	species	ref
staged	MurA·UDP-MurNAc·HPO_3H^-	12	3ISS	*E. coli*	this work
	MurA·EP-UDP-GlcNAc·P_i	1	2YVW	*Aquifex aeolicus*	*46*
	MurA·UDP-GlcNAc·SO_4^{2-}	1	2RL1	*Haemophilus influenzae*	*19*
closed	MurA_C115A·FTHI	1	1A2N	*E. coli*	*13*
	MurA_D305A·THI	16	1Q3G	*Enterobacter cloacae*	*15*
	MurA_C115S·EP-UDP-GlcNAc·P_i	8	1RYW	*En. cloacae*	*16*
	MurA-fosfomycin·UDP-GlcNAc	1	1UAE	*E. coli*	*17*
	MurA-fosfomycin·UDP-GlcNAc·SO_4^{2-}	1	2RL2	*H. influenzae*	*19*
	MurA·cnicin-UDPGlcNAc adduct	4	2Z2C	*E. coli*	*20*
open	unliganded MurA	2	1DLG	*En. cloacae*	*12*
	unliganded type 2 MurA	1	1EJC	*En. cloacae*	*14*
	unliganded type 1 MurA	2	1EJD	*En. cloacae*	*12*
	MurA·ANS	1	1EYN	*En. cloacae*	*11*
	unliganded MurA	2	1NAW	*En. cloacae*	*2*
	MurA·5-sulfonoxyanthranilate	4	1YBG	*En. cloacae*	*18*

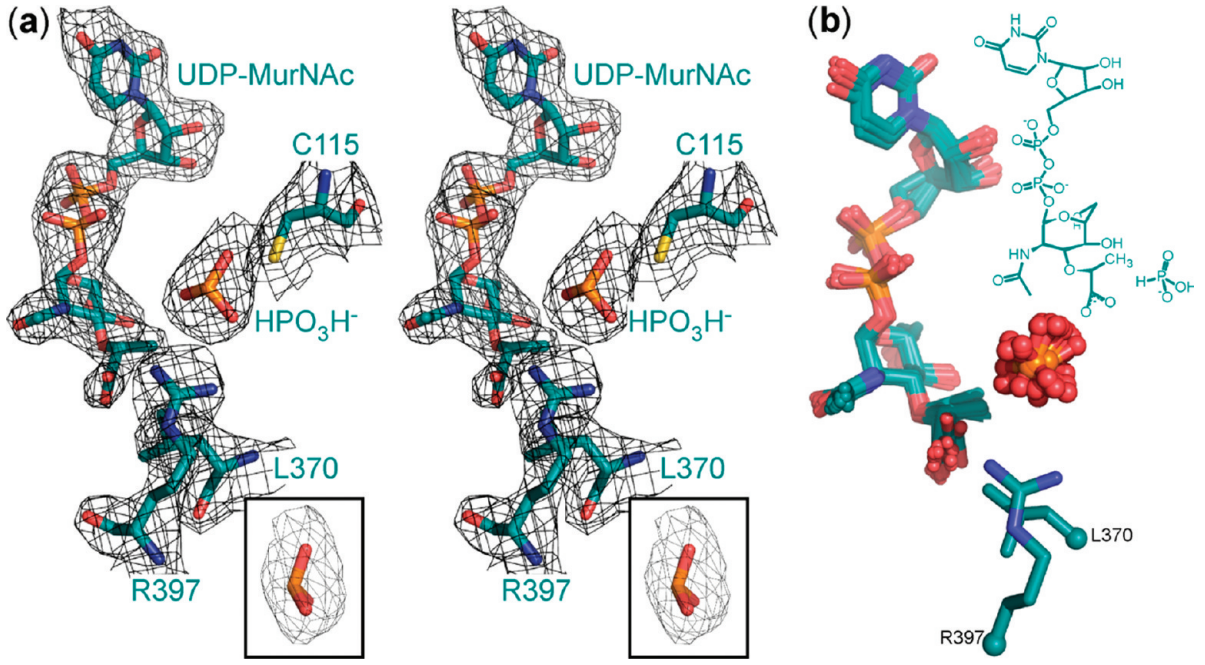

FIGURE 2: (a) Electron density of UDP-MurNAc, phosphite, C115, L370, and R397 from chain I. The inset shows a side view of phosphite, showing its flattened electron density. (b) UDP-MurNAc and phosphite ligands from all 12 superimposed molecules in the asymmetric unit.

To obtain quantitative, functional information about MurA's flexibility, its THI was tested as a substrate. Its breakdown was 3×10^5-fold slower than the corresponding AroA reaction (*23*). The nearly diffusion rate-limited reaction of AroA THI with AroA supports its kinetic competence; however, the converse observation, that MurA THI breakdown is slow, is not evidence against kinetic competence. Enzymes do not generally release catalytic intermediates into solution, so there is no specific requirement for fast rebinding (*43*). Rather, kinetic competence requires only that a true intermediate's reaction rate, once bound, must equal the overall catalytic rate (*8*). Thus, AroA and MurA are examples of the extremes of very fast and very slow reaction rates with their cognate intermediates.

In principle, slow MurA THI binding could arise from the protein conformation being predominantly closed in solution, and only occasionally opening. However, small-angle X-ray scattering showed a 10% larger radius of gyration for free MurA versus the MurA·UDP-GlcNAc complex, suggesting that the loop is predominantly open in solution (*5*). Thus, the slow observed rate was due to slow association of THI with MurA, evidence of the kinetic importance of MurA's limited conformational repertoire.

Cα atoms move by up to 19 Å in the conversion from MurA's open to closed conformations, but outside of this local change, Cα atoms in the active site cleft move by < 3 Å [PDB entry 1DLG (*12*) vs PDB entry 1Q3G (*15*)]. In contrast, the *E. coli* AroA domains open dramatically, by > 20 Å at the entrance to the active site [PDB entry 1EPS (*25*) vs PDB entry 1Q36 (*15*)].

The similarity of THI partitioning, with *f*(PEP) values of 0.22 for MurA and 0.25 for AroA (*23*), showed that once bound, both THIs are subject to similar catalytic forces, with THI breakdown being accelerated 8×10^4 to 1.5×10^5-fold (*29*, *33*, *35*). Nonenzymatic breakdown occurs exclusively by P_i departure (*33*), but both enzymes produce significant amounts of PEP, meaning that they catalyze R-OH departure more than P_i (Scheme 1).

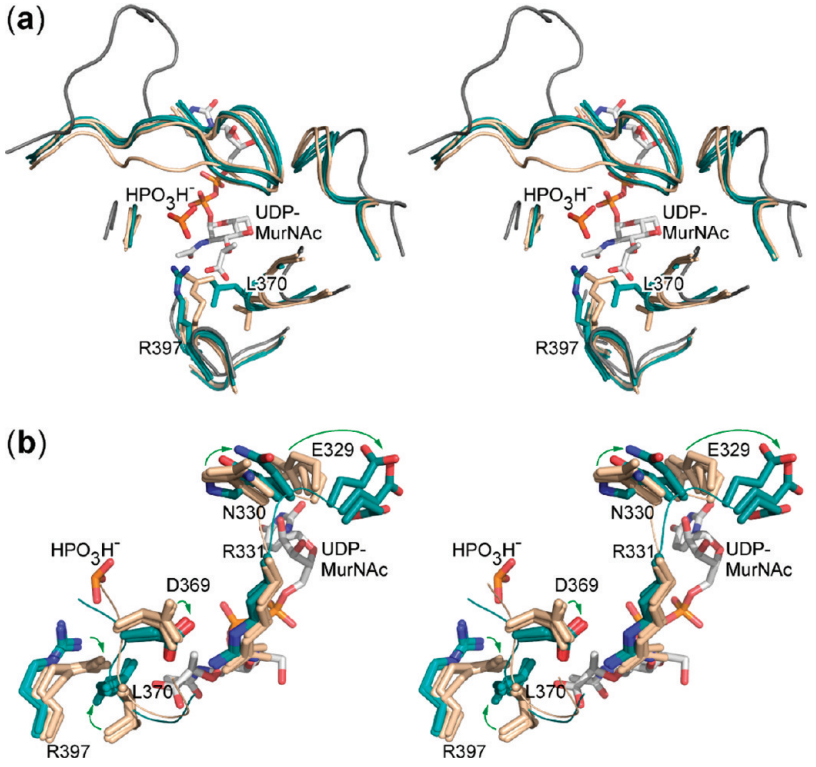

FIGURE 3: (a) Ribbon representation of the active site region of the three staged structures (teal), with three representative closed structures (beige) and one representative open conformation. UDP-MurNAc and phosphite are shown (white carbon atoms), along with the side chains of L370 and R397 from PDB entries 3ISS and 1A2N. (b) Catalytic site residues showing the closed (beige)-to-staged (teal) transition. Residues E329 and N330 are engaged in hydrogen bonds with the active site loop (not shown) in the closed structures. The closed structures are PDB entries 1A2N, 1RYW, and 2RL2, and the open structure is PDB entry 1DLG.

Scheme 3

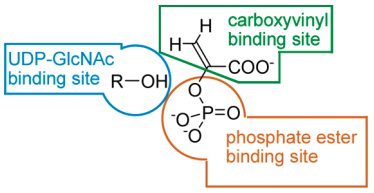

Protein Structure and Conformational Changes. (*i*) *MurA·UDP-MurNAc·Phosphite Structure*. The 12 molecules of the asymmetric unit of MurA·UDP-MurNAc·phosphite were almost identical, aside from some heterogeneity in solvent-exposed side chains. Superposition gave rmsds of 0.03−0.04 Å for Cα atoms, and the UDP-MurNAc residues were also closely superimposed (Figure 2b). The phosphite anion exhibited several distinct orientations. Given phosphite's pK_a values of 2.0 (*44*) and 6.6 (*45*), and the crystallization pH of 6.2, there were significant concentrations of both the monoanion and dianion forms in the crystallization buffer, i.e., 71% HPO_3H^- and 29% HPO_3^{2-}. The protonation state of the protein-bound phosphites is not known. There is some evidence from studies of phosphate analogues that at least one proton is required for binding in the phosphate ester binding site (*34*) (Scheme 3), though there is no evidence of the protonation state in the polyanion binding site (see below).

(*ii*) *Staged Conformation*. The MurA·UDP-MurNAc·-phosphite structure was superficially similar to the closed conformation; however, there were distinctive protein conformational changes around the carboxyvinyl binding site (Figure 3a and Figure S1 of the Supporting Information). The staged conformation was found in two further structures, *H. influenzae* MurA·UDP-GlcNAc·SO_4^{2-} (PDB entry 2RL1) (*19*) and *A. aeolicus* MurA·EP-UDP-GlcNAc·P_i (PDB entry 2YVW) (*46*) (Table 2). The sequence similarity between these structures was modest, 71 and 42% identical, compared with *E. coli* (Table S1 of the Supporting Information), but the active sites of the staged structures were more similar to each other than they were to any closed conformations (Figure 3b and Figure S2 of the Supporting Information).

The name "staged" highlights its characteristic feature, a polyanion binding site. Each staged structure has a polyanion (phosphite, P_i, or sulfate) bound in a "staging" site close to, but distinct from, the phosphate ester binding site (Figure 4). The staged conformation has a unique set of enzyme·ligand and intramolecular side chain interactions; it is not merely an intermediate state between the open and closed conformations.

(*iii*) *Closed Conformation*. There are six closed MurA structures complexed with substrate-like ligands (Table 2). The active site loop (P112−P121) caps the active site, forming a short tunnel. The catalytic site is in the middle, ~15 Å from the tunnel entrance. The beginning of the active site loop (P112−C115) is conformationally variable, possibly to allow C115 to approach PEP. The end of the loop (I117−P121) is less variable because of hydrogen bonds from T116, I117, and A119 to the C-terminal domain.[2]

(*iv*) *Open Conformation*. Six *En. cloacae* MurA structures have open conformations, with the active site cleft being solvent accessible. Four structures are unliganded, while two contain non-substrate-like ligands (Table 2).

[2]The N-terminal domain consists of residues G20−L229; the C-terminal domain consists of residues M1−S19 and P230−G418.

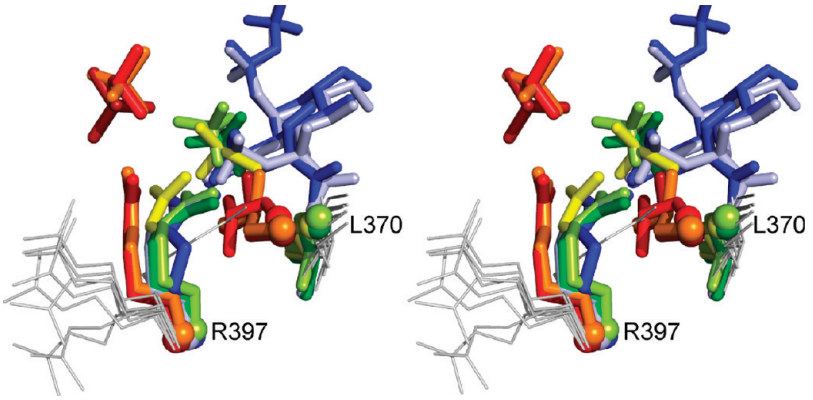

FIGURE 4: Polyanion binding site and R397 tracking. Staged conformation: red for 3ISS, dark red for 2YVW, and orange for 2RL1. Closed conformation: blue for 1A2N, light blue for 1Q3G, green for 1RYW, light green for 2RL2, and yellow for 1UAE. Open conformation: gray for 1DLG, 1EJC, 1EJD, 1EYN, 1NAW, and 1YBG. 2Z2C is not shown. It has a closed conformation but lacks a negative charge in the phosphate binding site. R397 is located between the staged and open conformations. FTHI (1A2N) and THI (1Q3G) are shown, plus the phosphonate ester group of the covalently modified C115 residue (1UAE).

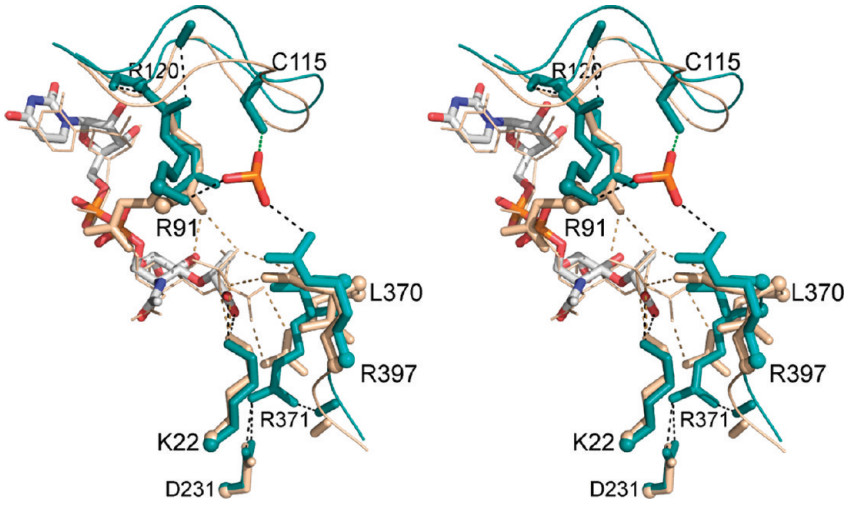

FIGURE 5: Comparison of staged (teal, 3ISS) vs closed (beige, 1A2N) conformations at the "bottom" of the active site.

Staged versus Closed Conformations. The closed-to-staged transition suggests a choreographed series of structural changes leading to product dissociation. The transition involves breaking 11 ion pairs or hydrogen bonds and forming 11 new ones. Of the 11 lost interactions, 8 involve MurA·ligand contacts, while 7 of the 11 new interactions are intraprotein.

The most obvious change is the R397 side chain "tracking" the polyanion ligand through the active site (Figure 4). In closed conformations, it forms an ion pair with the phosphate ester of FTHI (*13*) and THI (*15*),[3] with P_i in the closed MurA·EP-UDP-GlcNAc·P_i structure (*16*), with the phosphonate moiety of fosfomycin in the *E. coli* MurA-fosfomycin·UDP-GlcNAc structure (*17*), and the sulfate that occupies the phosphate binding site in the *H. influenzae* MurA-fosfomycin·UDP-GlcNAc·SO_4^{2-} structure (*19*). R397 was previously proposed to have a role in product dissociation on the basis of the conformational difference between the closed and open forms (*16*); the staged conformation specifically shows that it has a role in ion pairing with and tracking polyanion ligands.

As R397 tracks the departing anion, L370 moves into the space it vacates. This motion is propagated through D369 moving to form a new ion pair with R331 while two neighboring residues, E329 and N330, break their three hydrogen bonds with the active site loop, presumably allowing the loop to open.

Contacts with the carboxyvinyl group are lost in the closed-to-staged transition, including the bidentate C1 carboxylate·R371 ion pair (Figure 5). R371 forms a new bidentate ion pair with D231 and an ion−dipole interaction with the G398 C=O group. The UDP-MurNAc C1 carboxylate shifts into the phosphate ester binding site and makes two contacts with K22 Nε, compensating for the loss of two K22 Nε·phosphate ester contacts in the closed conformation. The R120 Nη·phosphate ester ion pair is also lost. These changes appear to be part of the process of product dissociation, but they are not essential for the formation of the staged conformation. The carboxyvinyl binding site of the MurA·UDP-GlcNAc·SO_4^{2-} structure is indistinguishable from the other two staged structures in spite of the lack of ligand atoms in the carboxyvinyl binding site.

The final large-scale change is the R91 side chain becoming ordered in the staged conformation. It is variable in the closed and open conformations, but ordered in the staged

[3]The MurA_D305A·THI structure (PDB entry 1Q3G) contains 16 molecules per asymmetric unit. In 8 of 16 molecules, R397 makes one contact with the THI phosphate, while it forms two contacts in 3 molecules, and no contacts in 5. This variability could be related to the nearby solvent ethylene glycol molecule perturbing the active site conformation. Figure 4 shows chain A, in which R397 makes one contact.

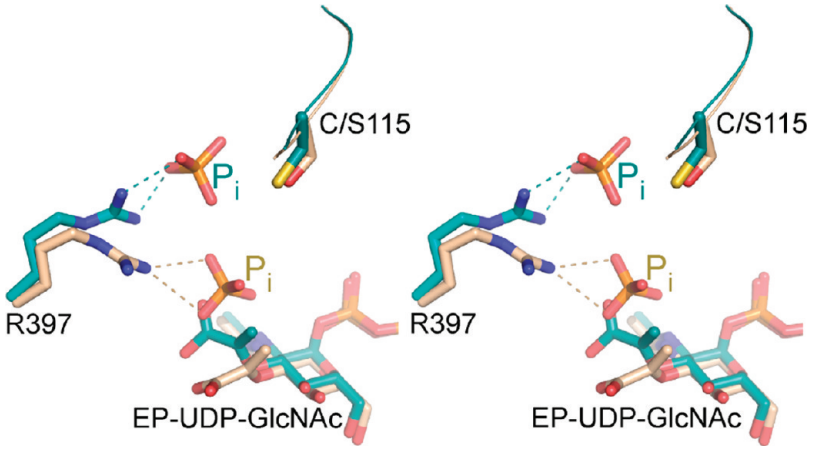

FIGURE 6: MurA·EP-UDPGlcNAc·P_i (teal, 2YVW) in the staged conformation compared with MurA_C115S·EP-UDPGlcNAc·P_i (beige, 1RYW) in the closed conformation.

conformation, forming ion−dipole interactions at opposite ends of the active site loop, with the backbone C=O group of G113 and R120.

(*i*) *Cys115 in the Staged Conformation*. C115 appears to play an essential but poorly defined role in product release. The C115S mutant of *En. cloacae* MurA was characterized in detail and appeared to be able to perform only a single cycle of catalysis (*16*), implying a deficiency in product release. Crystallization in the presence of the substrates UDP-GlcNAc and PEP yielded a closed conformation product complex, MurA_C115S·EP-UDP-GlcNAc·P_i (PDB entry 1RYW) (Figure 6) (*16*). In contrast, the wild-type *A. aeolicus* MurA·EP-UDP-GlcNAc·P_i complex (*46*) exists in the staged conformation. The degree of sequence identity between these MurAs is only 42%, but each structure's conformation is typical of its type, closed or staged, which is highly suggestive of C115's role in forming the staged conformation. How C115 controls conformation is not clear. It is in van der Waals contact with phosphite and sulfate in the staged structures, but it is 4.3 Å from P_i in *A. aeolicus* MurA·EP-UDP-GlcNAc·P_i; in any event, thiols are not good hydrogen bond donors or acceptors. The *E. coli* C115D mutant is active, and Asp is the only other naturally occurring amino acid at this position (*29*). It is not clear why Ser cannot play the same role in product release as Cys and Asp.

Whatever role C115 might play in product release, it would be consistent with its other previously proposed role as a general acid or base catalyst in protonating or deprotonating C3 during THI formation and breakdown (*29*). The chemical steps are complete before product dissociation begins, and C115 would be in the neutral, thiol form after THI breakdown; therefore, acid or base catalysis would be independent of C115 acting in product release.

(*ii*) *Staging Site*. The polyanion staging site is located in the tunnel leading from the catalytic site to the protein surface. There are three polyanion contacts in this site, namely, an ion pair with R397 Nη, an ion−dipole interaction with the R91 backbone NH group, and a van der Waals contact with C115 Sγ. Sulfate and phosphite make all three contacts, while P_i interacts with only R397 and R91. The staging site is surrounded by residues R91, R120, and R397, though only the R397 side chain makes direct contact with the polyanion (Figure 7).

P_i Staging in Product Release. Why would P_i bind in a staging site before final release? One possibility is that staged dissociation of P_i assists release of the EP-UDP-GlcNAc product.

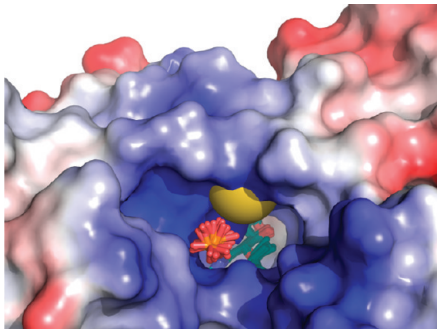

FIGURE 7: Electrostatic potential around phosphite. UDP-MurNAc is seen deep in the tunnel, and C115 Sγ is shown as a yellow sphere.

Tracking of the departing P_i by R397 is coupled with conformational changes throughout the active site. In total, eight enzyme·ligand contacts in the closed conformation are lost in the transition to a staged conformation, being "paid for" energetically by seven new intraprotein ion pairs or ion−dipole interactions.

Staged dissociation may also assist departure of P_i itself by permitting it to move away from the catalytic site without immediately breaking the R397·P_i ion pair, and by coupling its movement with the formation of new intraprotein contacts. P_i accelerates the chemical steps of catalysis $>5 \times 10^5$-fold (*34*). That is, it provides >7.7 kcal/mol of transition state stabilization, a significant fraction of the largest values, ~12 kcal/mol, observed for P_i (*47*). This implies tight P_i interactions during catalysis, and potentially the need to energetically couple its release with protein conformational changes.

The staged conformation is a snapshot of what appears to be a highly choreographed product release process. The staged-to-open transition likely involves R397 continuing to track P_i as it leaves the active site. Interruption of the choreography would result in the MurA·ligand complex being stalled, as observed in the slow dissociation of the MurA·UDP-GlcNAc (*31*) and MurA·UDP-MurNAc complexes (*3*), and the single-turnover reactions observed in the MurA_C115S mutant (*16*).

Contacts between UDP-MurNAc and MurA in the carboxyvinyl binding site region were not as one would have expected on the basis of closed conformation structures. In the future, it will be necessary to consider interactions in the staged conformation in designing MurA inhibitors.

CONCLUSIONS

Previous MurA crystal structures and other anecdotal evidence had suggested a limited conformational repertoire, and kinetic control of ligand dissociation. The extremely slow enzymatic breakdown of MurA THI demonstrated this functionally, and the crystal structure of the MurA·UDP-MurNAc·phosphite complex revealed a staged conformation. There is a shift from enzyme·ligand contacts in the closed conformation toward intraprotein contacts in the staged conformation, apparently as part of a choreographed product dissociation process.

SUPPORTING INFORMATION AVAILABLE

Additional structure figures and a table of amino acid sequence identities. This material is available free of charge via the Internet at http://pubs.acs.org.

REFERENCES

1. Hendlin, D., Stapley, E. O., Jackson, M., Wallick, H., Miller, A. K., Wolf, F. J., Miller, T. W., Chaiet, L., Kahan, F. M., Foltz, E. L., Woodruff, H. B., Mata, J. M., Hernandez, S., and Mochales, S. (1969) Phosphonomycin, a new antibiotic produced by strains of streptomyces. *Science 166*, 122–123.
2. Schonbrunn, E., Sack, S., Eschenburg, S., Perrakis, A., Krekel, F., Amrhein, N., and Mandelkow, E. (1996) Crystal structure of UDP-*N*-acetylglucosamine *enol*pyruvyltransferase, the target of the antibiotic fosfomycin. *Structure 4*, 1065–1075.
3. Mizyed, S., Oddone, A., Byczynski, B., Hughes, D. W., and Berti, P. J. (2005) UDP-*N*-acetylmuramic acid (UDP-MurNAc) is a potent inhibitor of MurA (*enol*pyruvyl-UDP-GlcNAc synthase). *Biochemistry 44*, 4011–4017.
4. Mengin-Lecreulx, D., Flouret, B., and van Heijenoort, J. (1982) Cytoplasmic steps of peptidoglycan synthesis in *Escherichia coli*. *J. Bacteriol. 151*, 1109–1117.
5. Schonbrunn, E., Svergun, D. I., Amrhein, N., and Koch, M. H. (1998) Studies on the conformational changes in the bacterial cell wall biosynthetic enzyme UDP-*N*-acetylglucosamine *enol*pyruvyltransferase (MurA). *Eur. J. Biochem. 253*, 406–412.
6. Gunetileke, K. G., and Anwar, R. A. (1968) Biosynthesis of uridine diphospho-*N*-acetylmuramic acid. II. Purification and properties of pyruvate-uridine diphospho-*N*-acetylglucosamine transferase and characterization of uridine diphospho-*N*-acetylenopyruvylglucosamine. *J. Biol. Chem. 243*, 5770–5778.
7. Marquardt, J. L., Siegele, D. A., Kolter, R., and Walsh, C. T. (1992) Cloning and sequencing of *Escherichia coli* murZ and purification of its product, a UDP-*N*-acetylglucosamine *enol*pyruvyl transferase. *J. Bacteriol. 174*, 5748–5752.
8. Marquardt, J. L., Brown, E. D., Walsh, C. T., and Anderson, K. S. (1993) Isolation and structural elucidation of a tetrahedral intermediate in the UDP-*N*-acetylglucoamine enolpyruvyl transferase enzymatic pathway. *J. Am. Chem. Soc. 115*, 10398–10399.
9. Lees, W. J., and Walsh, C. T. (1995) Analysis of the enol ether transfer catalyzed by UDP-GlcNAc *enol*pyruvyl transferase using (*E*)- and (*Z*)-isomers of phospho*enol*butyrate: Stereochemical, partitioning, and isotope effect studies. *J. Am. Chem. Soc. 117*, 7329–7337.
10. Samland, A. K., Jelesarov, I., Kuhn, R., Amrhein, N., and Macheroux, P. (2001) Thermodynamic characterization of ligand-induced conformational changes in UDP-*N*-acetylglucosamine *enol*pyruvyl transferase. *Biochemistry 40*, 9950–9956.
11. Schonbrunn, E., Eschenburg, S., Luger, K., Kabsch, W., and Amrhein, N. (2000) Structural basis for the interaction of the fluorescence probe 8-anilino-1-naphthalene sulfonate (ANS) with the antibiotic target MurA. *Proc. Natl. Acad. Sci. U.S.A. 97*, 6345–6349.
12. Schonbrunn, E., Eschenburg, S., Krekel, F., Luger, K., and Amrhein, N. (2000) Role of the loop containing residue 115 in the induced-fit mechanism of the bacterial cell wall biosynthetic enzyme MurA. *Biochemistry 39*, 2164–2173.
13. Skarzynski, T., Kim, D. H., Lees, W. J., Walsh, C. T., and Duncan, K. (1998) Stereochemical course of enzymatic enolpyruvyl transfer and catalytic conformation of the active site revealed by the crystal structure of the fluorinated analogue of the reaction tetrahedral intermediate bound to the active site of the C115A mutant of MurA. *Biochemistry 37*, 2572–2577.
14. Eschenburg, S., and Schonbrunn, E. (2000) Comparative X-ray analysis of the un-liganded fosfomycin-target MurA. *Proteins 40*, 290–298.
15. Eschenburg, S., Kabsch, W., Healy, M. L., and Schonbrunn, E. (2003) A new view of the mechanisms of UDP-*N*-acetylglucosamine *enol*pyruvyl transferase (MurA) and 5-*enol*pyruvylshikimate-3-phosphate synthase (AroA) derived from X-ray structures of their tetrahedral reaction intermediate states. *J. Biol. Chem. 278*, 49215–49222.
16. Eschenburg, S., Priestman, M., and Schonbrunn, E. (2005) Evidence that the fosfomycin target Cys115 in UDP-N-acetylglucosamine enolpyruvyl transferase (MurA) is essential for product release. *J. Biol. Chem. 280*, 3757–3763.
17. Skarzynski, T., Mistry, A., Wanacott, A., Hutchinson, S. E., Kelly, V. A., and Duncan, K. (1996) Structure of UDP-*N*-acetylglucosamine enolpyruvyl transferase, an enzyme essential for the synthesis of bacterial peptidoglycan, complexed with substrate UDP-*N*-acetylglucosamine and the drug fosfomycin. *Structure 4*, 1465–1474.
18. Eschenburg, S., Priestman, M. A., Abdul-Latif, F. A., Delachaume, C., Fassy, F., and Schonbrunn, E. (2005) A novel inhibitor that suspends the induced fit mechanism of UDP-N-acetylglucosamine enolpyruvyl transferase (MurA). *J. Biol. Chem. 280*, 14070–14075.
19. Yoon, H. J., Lee, S. J., Mikami, B., Park, H. J., Yoo, J., and Suh, S. W. (2008) Crystal structure of UDP-N-acetylglucosamine enolpyruvyl transferase from *Haemophilus influenzae* in complex with UDP-N-acetylglucosamine and fosfomycin. *Proteins 71*, 1032–1037.
20. Steinbach, A., Scheidig, A. J., and Klein, C. D. (2008) The Unusual Binding Mode of Cnicin to the Antibacterial Target Enzyme MurA Revealed by X-ray Crystallography. *J. Med. Chem. 51*, 5143–5147.
21. Anderson, K. S., and Johnson, K. A. (1990) Kinetic and structural analysis of enzyme intermediates: Lessons from EPSP synthase. *Chem. Rev. 90*, 1131–1149.
22. Steinrucken, H. C., and Amrhein, N. (1980) The herbicide glyphosate is a potent inhibitor of 5-enolpyruvyl-shikimic acid-3-phosphate synthase. *Biochem. Biophys. Res. Commun. 94*, 1207–1212.
23. Mizyed, S., Wright, J. E. I., Byczynski, B., and Berti, P. J. (2003) Identification of the catalytic residues of AroA (*enol*pyruvylshikimate 3-phosphate synthase) using partitioning analysis. *Biochemistry 42*, 6986–6995.
24. Anderson, K. S., and Johnson, K. A. (1990) "Kinetic competence" of the 5-enolpyruvoylshikimate-3-phosphate synthase tetrahedral intermediate. *J. Biol. Chem. 265*, 5567–5572.
25. Stallings, W. C., Abdel-Meguid, S. S., Lim, L. W., Shieh, H.-S., Dayringer, H. E., Leimgruber, N. K., Stegeman, R. A., Anderson, K. S., Sikorski, J. A., Padgette, S. R., and Kishore, G. H. (1991) Structure and topological symmetry of the glyphosate target 5-enol-pyruvylshikimate-3-phosphate synthase: A distinctive protein fold. *Proc. Natl. Acad. Sci. U.S.A. 88*, 5046–5050.
26. Park, H., Hilsenbeck, J. L., Kim, H. J., Shuttleworth, W. A., Park, Y. H., Evans, J. N., and Kang, C. (2004) Structural studies of *Streptococcus pneumoniae* EPSP synthase in unliganded state, tetrahedral intermediate-bound state and S3P-GLP-bound state. *Mol. Microbiol. 51*, 963–971.
27. Funke, T., Han, H., Healy-Fried, M. L., Fischer, M., and Schonbrunn, E. (2006) Molecular basis for the herbicide resistance of Roundup Ready crops. *Proc. Natl. Acad. Sci. U.S.A. 103*, 13010–13015.
28. Marquardt, J. L., Brown, E. D., Lane, W. S., Haley, T. M., Ichikawa, Y., Wong, C. H., and Walsh, C. T. (1994) Kinetics, stoichiometry, and identification of the reactive thiolate in the inactivation of UDP-GlcNAc *enol*pyruvoyl transferase by the antibiotic fosfomycin. *Biochemistry 33*, 10646–10651.
29. Kim, D. H., Lees, W. J., Kempsell, K. E., Lane, W. S., Duncan, K., and Walsh, C. T. (1996) Characterization of a Cys115 to Asp substitution in the *Escherichia coli* cell wall biosynthetic enzyme UDP-GlcNAc *enol*pyruvyl transferase (MurA) that confers resistance to inactivation by the antibiotic fosfomycin. *Biochemistry 35*, 4923–4928.
30. De Smet, K. A., Kempsell, K. E., Gallagher, A., Duncan, K., and Young, D. B. (1999) Alteration of a single amino acid residue reverses fosfomycin resistance of recombinant MurA from *Mycobacterium tuberculosis*. *Microbiology 145*, 3177–3184.
31. Brown, E. D., Marquardt, J. L., Lee, J. P., Walsh, C. T., and Anderson, K. S. (1994) Detection and characterization of a phospholactoyl-enzyme adduct in the reaction catalyzed by UDP-*N*-acetylglucosamine enolpyruvoyl transferase, MurZ. *Biochemistry 33*, 10638–10645.
32. Clark, M. E., and Berti, P. J. (2007) Enolpyruvyl Activation by Enolpyruvylshikimate-3-phosphate Synthase. *Biochemistry 46*, 1933–1940.

33. Byczynski, B., Mizyed, S., and Berti, P. J. (2003) Nonenzymatic breakdown of the tetrahedral (α-carboxyketal phosphate) intermediates of MurA and AroA, two carboxyvinyl transferases. Protonation of different functional groups controls the rate and fate of breakdown. *J. Am. Chem. Soc. 125*, 12541–12550.
34. Zhang, F., and Berti, P. J. (2006) Phosphate analogues as probes of the catalytic mechanisms of MurA and AroA, two carboxyvinyl transferases. *Biochemistry 45*, 6027–6037.
35. Berti, P. J., and Chindemi, P. (2009) Catalytic Residues and an Electrostatic Sandwich That Promote Enolpyruvyl Shikimate 3-Phosphate Synthase (AroA) Catalysis. *Biochemistry 48*, 3699–3707.
36. Webb, M. R. (1992) A continuous spectrophotometric assay for inorganic phosphate and for measuring phosphate release kinetics in biological systems. *Proc. Natl. Acad. Sci. U.S.A. 89*, 4884–4887.
37. Pflugrath, J. W. (1999) The finer things in X-ray diffraction data collection. *Acta Crystallogr. D55*, 1718–1725.
38. McCoy, A. J., Grosse-Kunstleve, R. W., Adams, P. D., Winn, M. D., Storoni, L. C., and Read, R. J. (2007) Phaser crystallographic software. *J. Appl. Crystallogr. 40*, 658–674.
39. Adams, P. D., Grosse-Kunstleve, R. W., Hung, L. W., Ioerger, T. R., McCoy, A. J., Moriarty, N. W., Read, R. J., Sacchettini, J. C., Sauter, N. K., and Terwilliger, T. C. (2002) PHENIX: Building new software for automated crystallographic structure determination. *Acta Crystallogr. D58*, 1948–1954.
40. Emsley, P., and Cowtan, K. (2004) Coot: Model-building tools for molecular graphics. *Acta Crystallogr. D60*, 2126–2132.
41. Thomas, A. M., Ginj, C., Jelesarov, I., Amrhein, N., and Macheroux, P. (2004) Role of K22 and R120 in the covalent binding of the antibiotic fosfomycin and the substrate-induced conformational change in UDP-N-acetylglucosamine enolpyruvyl transferase. *Eur. J. Biochem. 271*, 2682–2690.
42. Krekel, F., Oecking, C., Amrhein, N., and Macheroux, P. (1999) Substrate and inhibitor-induced conformational changes in the structurally related enzymes UDP-N-acetylglucosamine enolpyruvyl transferase (MurA) and 5-enolpyruvylshikimate 3-phosphate synthase (EPSPS). *Biochemistry 38*, 8864–8878.
43. Cleland, W. W. (1990) Kinetic competence of enzymic intermediates: Fact or fiction? *Biochemistry 29*, 3194–3197.
44. Kolthoff, I. M., Elving, P. J., and Editors (1959) Treatise on Analytical Chemistry .
45. Bjerrum, J., Schwarzenbach, G., Sillen, L. G., Berecki-Biedermann, C., Maltesen, L., Rasmussen, S. E., and Rossotti, F. J. C. (1958) Stability constants of metal-ion complexes, with solubility products of inorganic substances. II. Inorganic ligands with solubility products of inorganic substances , Vol. 7, Chemical Society, London.
46. Kitamura, Y., Yokoyama, S., and Kuramitsu, S. (2007) Crystal structure of UDP-N-acetylglucosamine 1-carboxyvinyltransferase from *Aquifex aeolicus* VF5. RIKEN Structural Genomics/Proteomics Initiative (RSGI): Protein Data Bank entry 2YWV (to be published).
47. Morrow, J. R., Amyes, T. L., and Richard, J. P. (2008) Phosphate Binding Energy and Catalysis by Small and Large Molecules. *Acc. Chem. Res. 41*, 539–548.